

Siloxane-based thin films for corrosion protection of stainless steel in chloride media

Sérgio Meth · Natali Savchenko · Federico A. Viva ·
David Starosvetsky · Alec Groysman ·
Chaim N. Sukenik

Received: 17 May 2010/Accepted: 17 March 2011/Published online: 3 July 2011
© Springer Science+Business Media B.V. 2011

Abstract The corrosion protection of stainless steel (SS 316L) provided by layers of SiO_2 and by siloxane-anchored self-assembled monolayer (SAMs) was assessed by cyclic voltammetry (CV) and by potentiostatic current transient in sodium chloride media. The SAMs were composed of octadecyltrimethoxysilane anchored onto a thin (1–2 nm) layer of SiO_2 . The initial SiO_2 layer was obtained by treatment with tetraethoxyorthosilicate. Successive layers were added by applying the alkylsiloxane and then oxidatively removed by treatment using a UV-ozone cleaner. Though SAMs have been used as corrosion barriers in other contexts, it is shown that successive cycles of SAM deposition and ablation provide an extended SiO_2 thin-covering layer that protects stainless steel against pitting and general corrosion.

Keywords Corrosion barrier coatings · 316L stainless steel · Self assembled monolayer · Pitting corrosion · Potentiostatic current transient

1 Introduction

Stainless steel is a material well known for its high corrosion resistance due to passive film formation [1, 2]. The passive film (composed mainly of chromium oxide) remains stable and inert over a wide pH range [3, 4]. The combination of excellent corrosion resistance, good mechanical properties, and an aesthetically pleasing appearance has made stainless steel as the material of choice for a diverse range of applications [2, 5]. However, stainless steel can undergo chemical attack in acidic solutions, such as HCl, HBr, HF, and some organic acids (formic, acetic, oxalic, and lactic). Surface reactivity has also been observed for oxidizing chlorides (FeCl_3 , HgCl_2 , CuCl_2 , NaOCl , etc.), seawater, and photographic solutions containing thiosulfates [6]. Depending on the environment, chemical composition, and heat treatment, stainless steel can undergo different types of localized corrosion: active dissolution, pitting corrosion, intergranular corrosion, stress corrosion cracking, or microbiologically induced corrosion [7, 8]. Pitting corrosion is particularly prominent in chloride ion-containing solutions [2, 6].

Siloxane-anchored self-assembled monolayer (SAM) films have attracted enormous interest [9–13] as surface modifiers since the study on them by Sagiv in 1980 [14]. They are composed of molecules that organize spontaneously by chemisorption from solution onto an appropriate substrate. This results in more stable films than those obtained by physisorbed Langmuir–Blodgett (LB) [15], despite being comparative thin. This improved stability allows SAMs for being employed in a broad range of applications [16, 17] including protection of metals against corrosion [18–22]. Since SAM can form a densely packed thin film, they can improve the anti-corrosive properties of metallic surfaces. For example, an alkylthiol monolayer is

S. Meth (✉) · C. N. Sukenik
Department of Chemistry, Bar Ilan University,
52900 Ramat Gan, Israel
e-mail: meth@usc.edu

N. Savchenko · A. Groysman
Oil Refineries Ltd, R&D Laboratory, 32000 Haifa, Israel

S. Meth · F. A. Viva
Department of Chemistry, Loker Hydrocarbon Research Institute, University of Southern California, Los Angeles, CA 90089, USA

D. Starosvetsky
Technion, 32000 Haifa, Israel

known to be effective in blocking electrochemical processes on copper surfaces [19, 23–27]. However, on rough surfaces like stainless steel with its natural corrosion resistance (i.e., the Cr₂O₃ passive layer), SAMs are typically not completely pore-free [28–30]. In order for SAM protection to be truly effective on stainless steel, it should protect not only against general corrosion, but also against pitting corrosion. In a different approach to corrosion resistance, sol-gel deposited SiO₂ has been applied as a protective coating on stainless steel [31–36]. However, annealing at high-temperatures (~800 °C) is required to obtain a well-defined crystalline structure of the oxide. Such high temperature exposure can be problematic since it can modify the crystalline structure and mechanical properties of the stainless steel [37, 38]. There are also reports of SiO₂ films regarding the protection of mild steel [39]; however, there is no indication in the literature of either SiO₂ thin films or siloxane-based SAM regarding protection of stainless steel.

We have previously reported [30] a process for obtaining octadecyltrimethoxysilane (OTMS) SAM on stainless steel by pre-coating the substrate with SiO₂ created by hydrolyzing tetraethoxyorthosilicate (TEOS) to provide an anchoring layer. Further, recently we have described the use of SiO₂-SAM to anchor TiO₂ for stainless steel protection [29]. It has also been reported that a compact SiO₂ layer can be created by “burning off” an OTMS monolayer [40, 41]. By this approach, oxidation of the SAM improves the coverage of the SiO₂ layer created by TEOS hydrolysis over stainless steel. Furthermore, the SiO₂ layer can serve as a base for a new layer of OTMS. Repeated application of this cycle results in a layer-by-layer growth of the oxide film, slowly increasing the thickness of the SiO₂ layer and extending the surface coverage. The enhanced layer of SiO₂ also improves the quality of the SAM that is deposited on it, making it a more compactly packed monolayer.

This study evaluates the use of a SAM as a protective film on stainless steel in chloride ion-containing solution. It uses both cyclic voltammetry (CV) and potentiostatic current transient methods to evaluate the corrosion-protective capability of SAMs anchored to the initial SiO₂-based layer and SAMs deposited on extended SiO₂ layer obtained by SAM oxidation with an UV-ozone cleaner. It also attempts to define the degree to which corrosion protection is afforded by the SiO₂ layers or by the organic SAM films.

2 Experimental details

2.1 General

All the reagents and solvents were obtained (unless otherwise specified) from Aldrich Chemical Co. and used

as received. Water was deionized and then distilled in an all-glass apparatus. Dicyclohexane (DCH) was purchased from Fluka, and was vacuum-distilled before use. Octadecyltrimethoxysilane (OTMS) was purchased from Aldrich and distilled under vacuum before use. Chloroform, acetone, and ethanol (all AR grade) were purchased from Biolab, and were used as received.

2.2 Sample preparation

All the synthesis and surface modification studies were carried out as previously reported [30]. In brief, stainless steel 316L (SS 316L) samples (5 × 2 cm) were polished to a mirror-like surface and coated with a thin layer of sol-gel-deposited SiO₂ obtained by the immersion of the stainless steel substrates in neat tetraethoxyorthosilicate (TEOS), followed by immersion in DCH. The SiO₂ deposition by TEOS adds a layer on top of the stainless steel without organic residue as was observed using FTIR and XPS [30]. This initial deposition of SiO₂ onto stainless steel was then used as the anchoring layer for the SAM growth. The SAM is deposited from a stirred solution of 2 mM of OTMS in DCH. After 30 min, two drops of glacial acetic acid were added, and the solution was heated at 60 °C for 15 min. The samples were kept in the stirred solution for an additional 48 h at room temperature. During the whole process, there was no care taken to avoid humidity from the air. After coating, the samples were cleaned for 30 min in chloroform on an ultrasonic bath.

The creation of the extended SiO₂ layer involved treating the OTMS-coated surface for 2 h in a UV-ozone cleaner (UVOCS/Model T10X10/OES/E, UVOCS Inc., Montgomeryville, PA), with the surface to be treated turned upward. Samples were then removed and put in distilled water for at least 10 min. The coating with OTMS/DCH was then repeated as described above. A simplified description of these steps is shown in Fig. 1, indicating how the oxidation by UV-ozone clearer increases the SiO₂ coverage of the stainless steel substrate.

2.3 Surface analysis

Analytic procedures have been described in detail elsewhere [30]. In brief, contact angle values were measured using a Rame-Hart Model 100 Contact Angle Goniometer. SiO₂ deposits and SAM film thickness were determined by ellipsometry using an M-44 ellipsometer (J.A. Woolam Co) using WVASE3 software, after calibration with a 25.0 nm SiO₂ on Si sample as a reference. Data were collected at take-off angles of 60, 65, and 70° and at 44 wavelengths between 624 and 1109 nm. Thickness measurement accuracy was ±2 nm. The ellipsometrically determined thicknesses were compared to theoretical values calculated

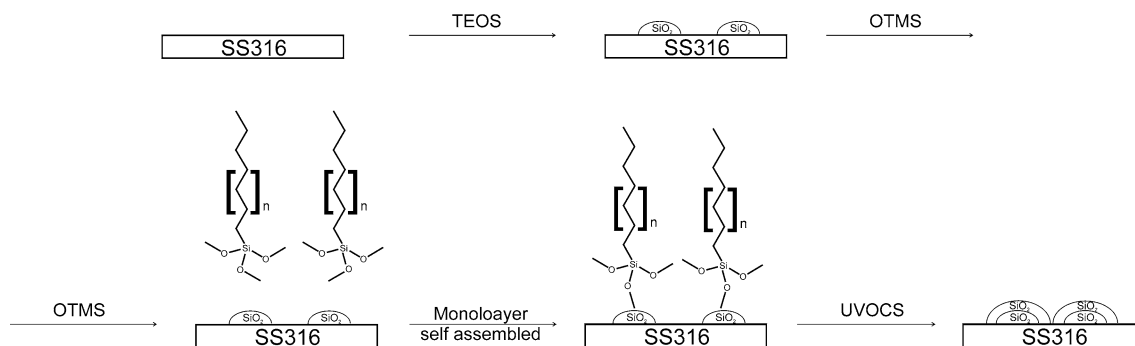


Fig. 1 Main steps in the process of obtaining the SAM and extending the SiO_2 layer by UV-ozone treatment

using the simplifying assumptions of the monolayer being perpendicular to the substrate and alkyl chains in an extended, all-trans conformation, with standard bond angles and lengths. Optical microscope image was obtained using an Olympus BX60 microscope coupled to a Nikon Cool-Pix 990 digital camera. SEM images of the stainless steel with its SiO_2 coatings were obtained using a JSM-840 JEOL instrument, previously coated by gold sputtering.

2.4 Electrochemical measurements

Electrochemical determinations were carried out in a 0.5 M NaCl aqueous solution, previously deaerated with N_2 , at $25 \pm 1^\circ\text{C}$ in a three-electrode electrochemical cell. A saturated calomel electrode (SCE) was used as reference electrode (RE) while a platinum wire (0.5 mm dia. \times 10 cm long AlfaAesar) was used as counter electrode (CE) [42–44]. Cell compartment for the RE was connected to the working electrode (WE) compartment through a Luggin capillary. All the electrochemical measurements were performed using a Gamry PC 4/750 potentiostat and Gamry ESA400TM (Electrochemical Signal Analyser) software.

The corrosion potential (E_{corr}) of the substrates with and without monolayer (4 cm^2 exposed area) were measured in the tested solution for 12 h. After this period, a potential sweep was applied with a scan rate of 1 mV s^{-1} , starting at a potential of 200–300 mV more negative than the measured E_{corr} and up to a potential in which the anodic current density (j) reached a value of 1 mA cm^{-2} [44]. Voltammograms are presented in the Tafel form [Potential (V) vs. $\log(j)$].

Current transients were measured potentiostatically [45] for a period of 20 min in steps of +100 mV versus E_{corr} up to a potential where continuous increase of current is present, indicating the occurrence of stable pitting. The samples were also exposed to the NaCl solution for 12 h at the same open circuit condition as in previous transient measurements.

3 Results and discussion

The thickness determined by ellipsometry of the SiO_2 layer on the stainless steel samples obtained after the initial TEOS treatment was 1.9 nm. Ellipsometric determination of the SAM thickness obtained on top of this base-layer presented a value of 2.4 nm for the monolayer as expected from an extended alkyl chain, indicative of molecules being organized approximately orthogonal to the surface. Determination of contact angles yielded a value of $117^\circ \pm 2^\circ$ for the advancing angle and $101^\circ \pm 3^\circ$ for the receding angle, also consistent with that of an extended alkyl chain monolayer [30, 46]. The samples with the enhanced SiO_2 layer had SiO_2 thickness 2.6 nm (i.e., an increase of 0.5 nm in SiO_2 thickness), and the SAM obtained on top the enhanced SiO_2 layer also presented a thickness of 2.4 nm. Figure 2 shows a stainless steel sample before and after deposition of SiO_2 by TEOS. Figure 2a presents a digital image from an optical microscope for the surface of the stainless steel after polishing, while fig. 2b shows the SEM image of the stainless steel after depositions of SiO_2 , where deposits of SiO_2 in the form of islands are evident.

Figure 3 presents the voltammograms of freshly polished SS 316L and SS 316L coated with SiO_2/SAM (SS/ SiO_2/SAM) in 0.5 N NaCl solution. The onset of anodic current was detected on SS/ SiO_2/SAM at a more positive potential value (+0.134 V) than that of the polished SS electrode (−0.27 V). The large region of passivity could be clearly seen in anodic curves obtained at positive potential sweep for both samples. The breakdown potential (E_p) for polished SS 316L was detected at a value ca. +0.4 V while that for SS/ SiO_2/SAM was ca. +0.5 V. The pits initiated at breakdown underwent repassivation (E_{rp}) at ca. +0.12 V in the case of the coated sample and at ca. +0.23 V in the case of polished SS. Current spikes appearing at potentials below breakdown in the anodic scan can be attributed to the metastable pits nucleation and repassivation for the

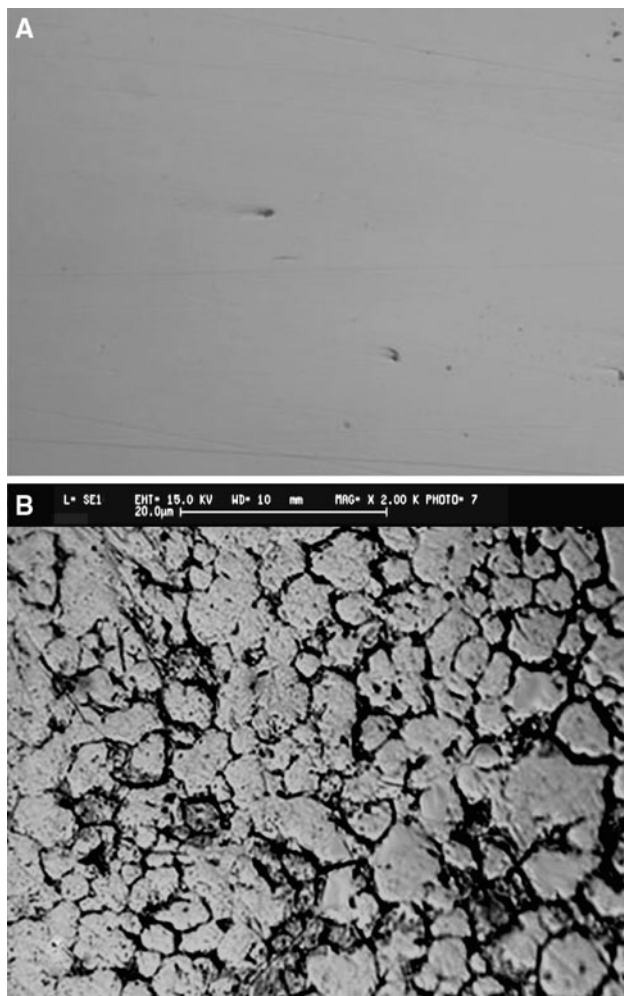


Fig. 2 **a** Optical microscope image of stainless steel after polishing. **b** SEM micrograph of stainless steel after SiO₂ deposition with TEOS

SS/SiO₂/SAM. The main difference in the corrosion behaviour of coated SS 316L versus uncoated SS 316L is the much lower corrosion current value measured in the region of steel passivity (approx. two orders of magnitude) with coated stainless steel sample. However, the presence of spikes and the close value of breakdown potential, together with the higher repassivation potential for polished SS indicated that the obtained SiO₂/SAM coverage is not enough for an efficient corrosion protection against pitting corrosion attack.

To increase the corrosion protection, the SiO₂-based-layer was subjected to the UV-ozone process which enhances the coverage of the SiO₂ layer. Over this enhanced SiO₂ layer a new SAM of OTMS was then deposited. The corrosion potential transients of SS 316L electrodes coated with OTMS over the enhanced SiO₂ layers showed an E_{corr} value of ca. +0.17 V, being more positive than those of the uncoated one and than those with the minimal coating, i.e. an OTMS monolayer on the enhanced SiO₂-based layer improved the passivity of a SS 316L electrode while the more simple coating of SiO₂/SAM did not present such improvement. Figure 4 shows the Tafel plots in 0.5 N NaCl solution for the polished SS and with the OTMS monolayer (2.10 nm) on the enhanced SiO₂ layer (2.5 nm). Without coating, the stainless steel remained passive in the potential range below +0.5 V where the pitting corrosion was nucleated. The initiated pits became re-passivated at -0.25 V. Unlike bare steel, the samples coated with OTMS on enhanced SiO₂ were passive over a much wider potential range (up to +1.05 V), and the current values in the region of passivity were markedly lower. In addition, the re-passivation voltage (-0.15 V) is more anodic than the corrosion potential

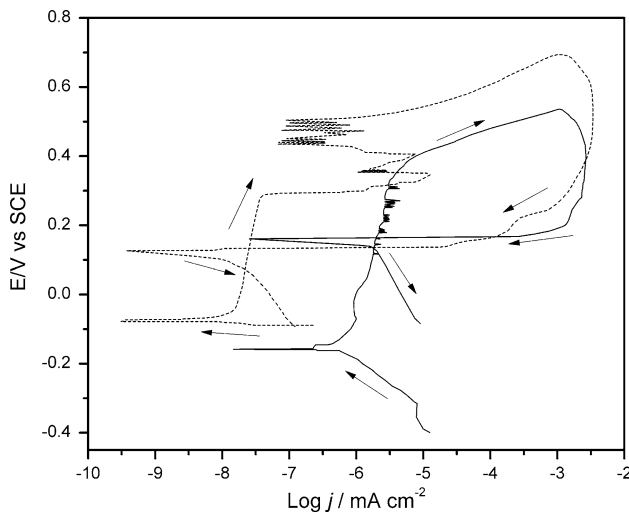


Fig. 3 Tafel plots for stainless steel 316L samples in 0.5 N NaCl. Freshly polished stainless steel (*solid lines*). SiO₂/SAM-covered stainless steel (*dashed lines*)

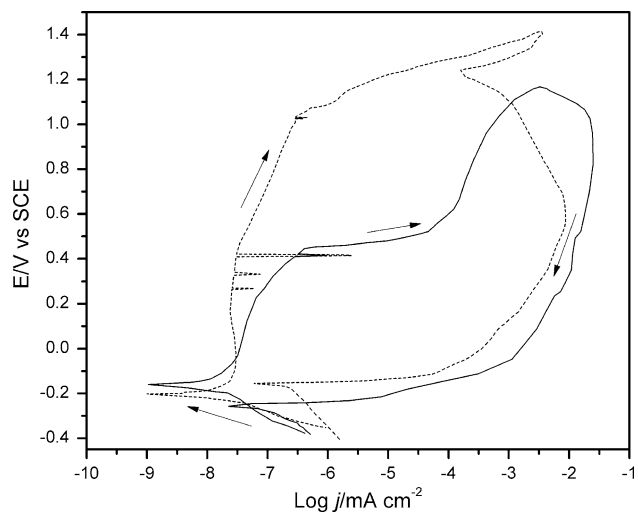


Fig. 4 Tafel plots for stainless steel 316L samples in 0.5 N NaCl. Freshly polished stainless steel (*solid lines*). Enhanced SiO₂/SAM-covered stainless steel (*dashed lines*)

(-0.2 V) for the stainless steel with SAM on enhanced SiO_2 . This behavior is not shown for the polished SS when the scan is reversed at a high anodic potential (>1.0 V), suggesting that the SAM/ SiO_2 on covered SS is harder to oxidize than the bare SS.

The results of the potentiostatic current transient measurements for the polished SS 316L, both with bare and with an enhanced SiO_2 layer, are depicted in Fig. 5. Potentials were referenced to the SCE in order to have a common origin. Uncoated SS samples remained passive at potentiostatic exposure up to ca. +400 mV (vs. SCE). Stable pit formation on the uncoated samples was obtained during exposure to +530 mV versus SCE (Fig. 4a). The increase of anodic current on the electrodes coated with OTMS on an enhanced SiO_2 layer was detected only when the applied potential was +770 mV versus SCE (Fig. 4b) indicating a higher resistance against pitting corrosion. This result for the potentiostatic current transient together with the one showed on the voltammograms indicates that the SAM on the enhanced SiO_2 layer provides a better protection against pitting corrosion than the more simple SiO_2 /SAM coverage.

Having seen that SAMs of comparable thickness gave significantly different corrosion protection depending on

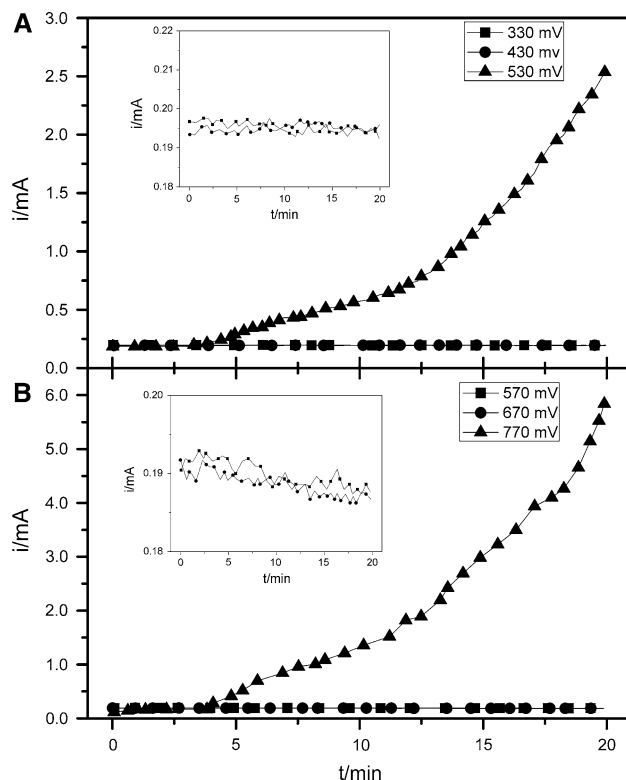


Fig. 5 Potentiostatic current transients records in 0.5 N NaCl at different potentials vs. SCE. **a** Freshly polished stainless steel sample. **b** Enhanced SiO_2 /SAM-covered stainless steel. Inset shows the potentials before the occurrence of corrosion



Fig. 6 SEM micrograph of a stainless steel sample after oxidation of two consecutive SAM layers

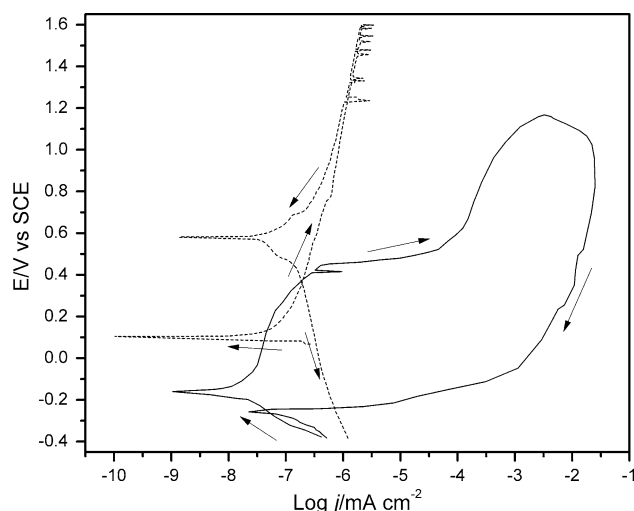


Fig. 7 Tafel plots for stainless steel 316L samples in 0.5 N NaCl. Freshly polished stainless steel (solid lines). Enhanced SiO_2 -layer covered stainless steel after oxidation of two consecutive SAM layers (dashed lines)

the underlying SiO_2 , it was reasonable to test whether the increased protection was due to the combination of the enhanced SiO_2 with the SAM or to the enhanced SiO_2 alone. To test this, a sample of SS with enhanced SiO_2 /SAM was treated again in the UV-ozone cleaner, burning off the SAM and providing a surface covered only by SiO_2 . This final removal of OTMS also added approx. 0.4 nm to the SiO_2 thickness resulting in a SiO_2 layer of 3 nm. The SEM image of the aforementioned covered sample is presented in Fig. 6. The image shows a more extended covered surface than the surface obtained with the TEOS-deposited SiO_2 (Fig. 2b). Figure 7 shows the Tafel plot of the stainless steel sample after the removal of OTMS. It can be observed that OTMS removal did not reduce the corrosion resistance of stainless steel samples. Moreover, these samples showed much more stable

passivity compared with the samples coated with the SAM on the enhanced SiO_2 layer. No breakdown of passivity was detected over the entire potential range up to +1.6 V versus SCE, corrosion shifted to more anodic potential when compared to the previously tested SS/ SiO_2 /SAM, and the repassivation potential also moved to more positive values. Overall, the samples (with extra increased SiO_2 layer) without the OTMS, indicated better protection against pitting corrosion than with the organic monolayer present, even though the SiO_2 layer only increased minimally.

4 Conclusions

A procedure to extend the coverage of SiO_2 on stainless steel and OTMS SAM is presented and their effectiveness for corrosion protection of stainless steel 316L was assessed by cyclic voltammetry and potentiostatic current transients in chloride ions-containing media. The SAM coating obtained on the initial SiO_2 layer does not provide significant corrosion protection. However, if the coated sample is burned off by UV-ozone (leaving behind an enhanced SiO_2 layer) and coated again with OTMS, there is good protection not only against general corrosion but also against pitting corrosion. Moreover, when this second OTMS layer is removed by the UV-ozone treatment, the resulting SiO_2 layer demonstrates much better protection of the stainless steel against corrosion, indicating that the growth of the SiO_2 layer is primarily responsible for the protection. The improved resistance to corrosion might be attributed not only on the increased thickness of the SiO_2 layer but also to the fact that the coverage of that layer is being extended concealing gaps and crevasses which are weak points where the corrosion can initiate. The OTMS SAM followed by UV-ozone is therefore an effective means of extending and enhancing the coverage of a compact SiO_2 layer over the surface of stainless steel providing protection against corrosion.

Acknowledgment This work was supported by a Tashbiyyot Grant from the Israel Ministry of Science.

References

- Dillon CP (1995) Corrosion resistance of stainless steel. Marcel Dekker, Inc., New York
- Groysman A (2010) Corrosion for everybody. Springer, New York
- Bard AJ, Parsons R, Jordan J (eds) (1985) Standard potentials in aqueous solutions, International Union of Pure and Applied Chemistry (IUPAC). Marcel Dekker, Inc, New York/Basel
- Pourbaix M (1966) Atlas of electrochemical equilibria in aqueous solutions. Pergamon Press, Oxford
- Davis JR (ed) (1994) ASM Specialty Handbook: Stainless Steel. ASM International, Materials Park
- Revie RW (ed) (2000) Uhlig's corrosion Handbook. Wiley, NY
- Brenda J, Little JS (2007) Microbiologically influenced corrosion. Wiley, New York
- Sedriks AJ (1996) Corrosion of stainless steel. Wiley-Interscience Publication, New York, USA
- Aramaki K (2007) Corros Sci 49:1963–1980
- Fadeev AY, Kazakevich YV (2002) Langmuir 18:2665–2672
- Robertson JWF, Tiani DJ et al (2007) Langmuir 23:4651–4661
- Ulman A (1991) An Introduction to Ultrathin Organic Films - From Langmuir-Blodgett to Self-Assembly. Academic Press, San Diego
- Wang XJ, Hu WC et al (2003) Langmuir 19:9748–9758
- Sagiv J (1980) J Am Chem Soc 102:92–98
- Blodgett KB (1935) J Am Chem Soc 57:1007–1022
- Wu F, Hu Z et al (2008) Electrochim Acta 53:8238–8244
- Ruckenstein E, Li ZF (2005) Adv Colloid Interfac 113:43–63
- Rohwerder M, Grundmeier G et al (2002) Corros Technol 17:479–527
- Shimura T, Aramaki K (2008) Corros Sci 50:596–604
- Vaidya RU, Brozik SM et al (1999) Metall Trans A 30A: 2129–2134
- Wang DH, Ni YH et al (2005) Thin Solid Films 471:177–185
- Hintze PE, Calle LM (2006) Electrochim Acta 51:1761–1766
- Ishibashi M, Itoh M et al (1996) Electrochim Acta 41:241–248
- Itoh M, Nishihara H et al (1995) J Electrochem Soc 142:3696–3704
- Petrovic Z, Metikos-Hukovic M et al (2008) Prog Org Coat 61:1–6
- Guo WJ, Chen SH et al (2006) Electrochim Acta 52:108–113
- Taneichi D, Haneda R et al (2001) Corros Sci 43:1589–1600
- Lin H, Kozuka H et al (1998) Thin Solid Films 315:111–117
- Meth S, Savchenko N et al (2010) Corros Sci 52:125–129
- Meth S, Sukenik CN (2003) Thin Solid Films 425:49–58
- Atik M, De Lima Neto Petal (1995) J Appl Electrochem 25:142–148
- Fuentes-Gallego JJ, Blanco E et al (1997) Thin Solid Films 301:12–16
- Ballarre J, Jimenez-Pique E et al (2009) Surf Coat Tech 203:3325–3331
- Gallardo J, Durán A et al (2004) Corros Sci 46:795–806
- López DA, Rosero-Navarro NC et al (2008) Surf Coat Tech 202:2194–2201
- Shin DY, Kim KN et al (2006) Mater Sci Forum 510–511:442–445
- Trasatti SP, Camona E et al (1998) J Appl Electrochem 28:1333–1341
- Takemori M (2009) Ceram Int 35:1731–1746
- Vives S, Meunier C (2008) Surf Coat Tech 202:2374–2378
- Brunner H, Vallant T et al (1996) Langmuir 12:4614–4617
- Vallant T, Brunner H et al (2000) J Phys Chem B 104:5309–5317
- ASTM (2003) Standard test method for conducting cyclic potentiodynamic polarization measurements for localized corrosion susceptibility of Iron-, Nickel-, or Cobalt-Based Alloys. In: ASTM Standard G 61 Committee G01.11 on Electrochemical measurements in corrosion testing, Philadelphia, 2003
- ASTM (2004) Standard reference test method for making potentiostatic and potentiodynamic anodic polarization measurements. In: ASTM G5 Committee G01.11 on Electrochemical measurements in corrosion testing, Philadelphia, 2004
- Baboiyan R, Haynes GS (1981) Cyclic polarization measurements—experimental procedure and evaluation of test data, electrochemical corrosion testing, ASTM STP 727, USA
- Burstein GT, Pistorius PC et al (1993) Corros Sci 35:57–62
- Ruan C-M, Bayer T et al (2002) Thin Solid Films 419:95–104